Geometric and electronic structures of spiro-graphene comprising fused pentagons and octagons

Susumu Okada*, Nguyen Thanh Cuong, Yanlin Gao, and Mina Maruyama

Department of Physics, Graduate School of Pure and Applied Sciences, University of Tsukuba, 1-1-1 Tennodai, Tsukuba, Ibaraki 305-8571, Japan

Geometric and electronic structures of a two-dimensional covalent network, consisting of [5.5.5.5]-fenestratetraene and cyclooctatetraene frameworks, are studied, using density functional theory with the generalized gradient approximation. Because of these constituent units and their arrangement in a two-dimensional covalent network, this two-dimensional C allotrope has a metallic electronic structure with the Dirac nodal lines just below the Fermi level as in the case of other spiro-graphene materials. This C sheet is thermally stable and has a relatively high total energy of approximately 600 meV/atom with respect to that of graphene, which is close to other spiro-graphene materials, owing to its rippled covalent networks of sp^2 and sp^3 C atoms.

1. Introduction

Pairs of linear dispersion bands at the Fermi level and the K/K' point make graphene a unique material where unusual physical phenomena have been observed:[1–3] Electrons distributed through the honeycomb network lose their effective masses leading to an unusual quantum Hall effect and remarkable carrier mobility up to 200,000 $cm^2V^{-1}s^{-1}$.[4–7] Thus, graphene is regarded as an emerging material for investigating physical phenomena in low-dimensional science and designing functional devices in a wide area of modern technologies. In addition to these unique physical properties, the pairs of linear dispersion bands and the bipartite lattice symmetry cause further modulation in the electronic structure of graphene by imposing additional boundary conditions and by introducing structural imperfections. Atomic defects open a band gap or additional nonbonding states at the Fermi level in graphene, depending on the size, shape, and arrangement of defects.[8–13] Line imperfections lead to edges of graphene where peculiar edge localized states emerge when their edge contains the zigzag

*sokada@comas-tsukuba.jp

portions. Accordingly, strips of graphene possess semiconducting, metallic, and magnetic properties, depending on the edge shapes and width of the strips.[14–17] In addition to these atomic and line imperfections, topological imperfections, such as pentagons and heptagons, also cause unusual electronic structures to arise from the symmetry breaking of bipartite symmetry.[18–23]

Recent advances in polymerization techniques of small- and medium-sized hydrocarbon molecules permit tailoring of the network topology of π electrons on the covalent network of C atoms, where their size, shape, and dimensionality are precisely controlled. Graphene nanoribbons with unique edge shapes and nanoflakes have been synthesized by polymerizing planar hydrocarbon molecules and dendrimers with dehydrogenation on appropriate metal surfaces at an elevated temperature.[24–26] In addition to the molecules and dendrimers comprising sp^2 C atoms, hydrocarbon molecules containing sp^2 and sp^3 C atoms, such as iptycene and tetraphenylmethane, can form two- and three-dimensional covalent network materials with large pores that are capable of accommodating foreign atoms and molecules.[27–30] These materials possess unusual band structures near the Fermi level depending on the mutual arrangement of sp^2 moieties of the molecules, even though the π moieties are segmented by sp^3 C atoms.[31,32] Furthermore, two-dimensional networks with atomic thickness and nanometer-scale rippling (spiro-graphene) are proposed by embedding sp^3 C atoms into sp^2 networks with the form of a spiro-carbon structure, where the sp^3 atom is located at the vertex of four fused pentagons.[33–35] These spiro-graphene materials exhibit versatile electronic structures ranging from semiconducting to metallic with a Dirac nodal line, depending on the arrangement of the spiro-carbon units.

In this manuscript, we propose another spiro-graphene structure that has Dirac nodal lines near the Fermi level as the starting material for various derivatives that may possess unusual electronic structures. Using density functional theory (DFT) with the generalized gradient approximation, we found that the spiro-graphene consisting of [5.5.5.5]-fenestratetraene[36–39] and cyclooctatetraene frameworks, which are copolymerized in the network, is a metallic two-dimensional C allotrope with atomic thickness and structural rippling with a relatively high total energy with respect to graphene and good thermal stability. The mutual arrangement of spiro-carbon units makes the covalent network of the sp^2 moiety a bipartite network with respect to the sp^2 moiety of these constituent units. Accordingly, this spiro-graphene has Dirac nodal lines just below the Fermi level and along the middle and boundary of the two-dimensional Brillouin zone.

2. Calculation methods

All calculations in this work are performed using the DFT[40,41] implemented in the program packages STATE[42,43] and Quantum Espresso.[44] The generalized gradient approximation with the Perdew–Burke–Ernzerhof functional is adopted to describe the exchange-correlation potential energy of interacting electrons.[45] Interactions between electrons and nuclei are treated using an ultrasoft pseudopotential where the core radii are set to 1.5 bohr for both 2s and 2p valence states of the C atom.[46] The valence wave function and deficit charge density in the core region are expanded in terms of the plane wave basis sets with cut-off energies of 25 Ry and 225 Ry, respectively. Integration over the two-dimensional Brillouin zone was carried out using equidistant 4×4 $\boldsymbol{k}$-meshes, which were used for the self-consistent electronic structure calculations. Lattice parameters and internal atomic coordinates were optimized until the force acting on each atom became less than 5 mRy/Å.

3. Results and Discussion

The spiro-graphene has a copolymeric structure of [5.5.5.5]-fenestratetraene[36–39] and cyclooctatetraene [spiro-graphene(5,8)] (Fig. 1). Because of the two different orientations of sp^3 C atoms in the networks, the network contains two pairs of [5.5.5.5]-fenestratetraene and cyclooctatetraene units, leading to the bipartite structure with respect to both constituent units. These sp^3 C atoms also lead to the structural rippling of the two-dimensional C network material. The rippling is shallower than that of the spiro-graphene derived from spiro[4,4]nonatetraene because the constituent units contain larger sp^2 C moieties than that in the spiro-graphene comprising spiro[4,4]nonatetraene [spiro-graphene(5,0)]. The calculated total energy of this two-dimensional covalent network is 0.597 eV/atom higher than that of graphene under the optimum lattice parameters of $a = b = 10.6$ Å with the symmetry space group *Pmmn*. Although the network contains regular and distorted octagons in addition to fused pentagons, the total energy is close to that of other spiro-graphene materials.[33–35]

Table I shows the optimized atomic coordinates, optimized lattice parameters, and symmetry space group of the spiro-graphene(5,8). Because the network contains octagons, the spiro-graphene is a low atomic-density material with a density of 0.374 atom/Å^2, which is lower than those of the spiro-graphene(5,0) (0.411 atom/Å^2) and graphene (0.381 atom/Å^2). The optimized bond length associated with C6 is 1.496 Å with the bond angle of 94.78°. The bond length is slightly shorter and the angle is much narrower than those of ideal sp^3 C atoms. Therefore, the distorted nature of C6 substantially decreases the rippling while it increases the total energy. Bond lengths associated with sp^2 C atoms are 1.402, 1.455, 1.464, 1.397,

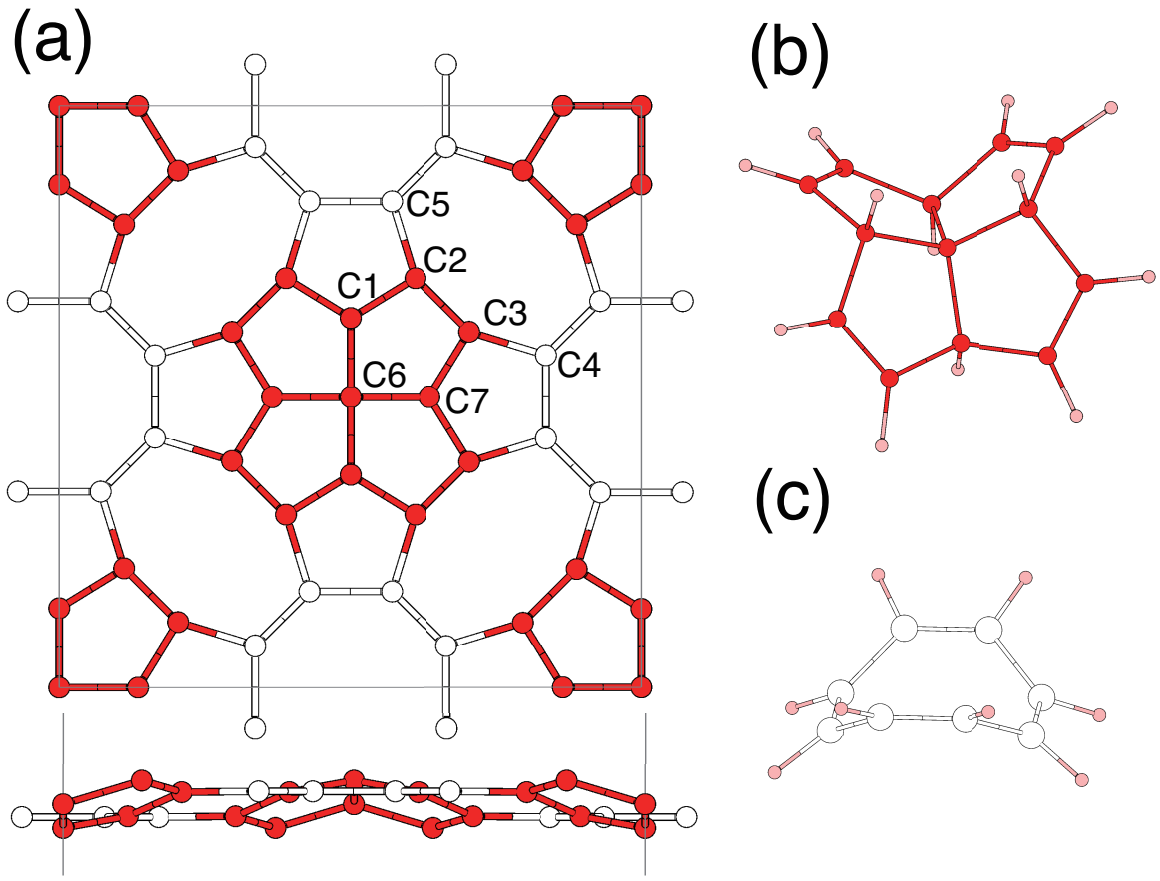

Fig. 1. (a) Top and side views of an optimized atomic structure of spiro-graphene comprising [5.5.5.5]-fenestratetraene and cyclooctatetraene frameworks. Red, white, and pink atoms indicate C atoms belonging to [5.5.5.5]-fenestratetraene, those belonging to cyclooctatetraene, and H atoms, respectively. The solid square indicates the unit cell boundary, and the indexes indicate independent atomic sites under the symmetry of *Pmmn*. Geometric structures of (b) [5.5.5.5]-fenestratetraene and (c) cyclooctatetraene.

and 1.504 Å for C1–C2/C7–C3, C2–C3, C3–C4/C2–C5, C4–C5, and C5–C5/C4–C4, respectively, with the bond angles ranging from 104.431° to 147.591°, indicating that the network is highly distorted from an ideal sp^2 covalent network. This large distortion may cause the higher total energy of the spiro-graphene than that of graphene.

It is necessary to investigate the thermal and dynamical stabilities of the spiro-graphene(5,8) by calculating the phonon dispersion relation. The phonon dispersion relation of the copolymer of [5.5.5.5]-fenestratetraene and cyclooctatetraene is evaluated using the finite displacement method implemented in the Phonopy code[47] with Quantum Espresso code [Fig. 2(a)] where a norm conserving pseudopotential for C atoms with cutoff energy of 60 Ry and the dense 6×6×1 Monkhorst-Pack $\boldsymbol{k}$-grid are adopted. Due to large number of atoms of the primitive cell, the 1×1×1 supercell is used for this phonon calculation. The calculated

Table I. Optimized atomic coordinates, lattice constants, and space group symmetry of the spiro-graphene comprising [5.5.5.5]-fenestratetraene and cyclooctatetraene units. Atom indexes are defined in Fig. 1.

Pmmn	$a = b$ =10.60 Å	c =12.00 Å	
C1	0.00000	0.86484	0.03599
C2	0.11124	0.79623	0.01834
C3	0.20376	0.88874	–0.01834
C4	0.33586	0.92906	–0.01952
C5	0.07093	0.66412	0.01952
C6	0.00000	0.00000	0.00000
C7	0.13515	0.00000	–0.03599

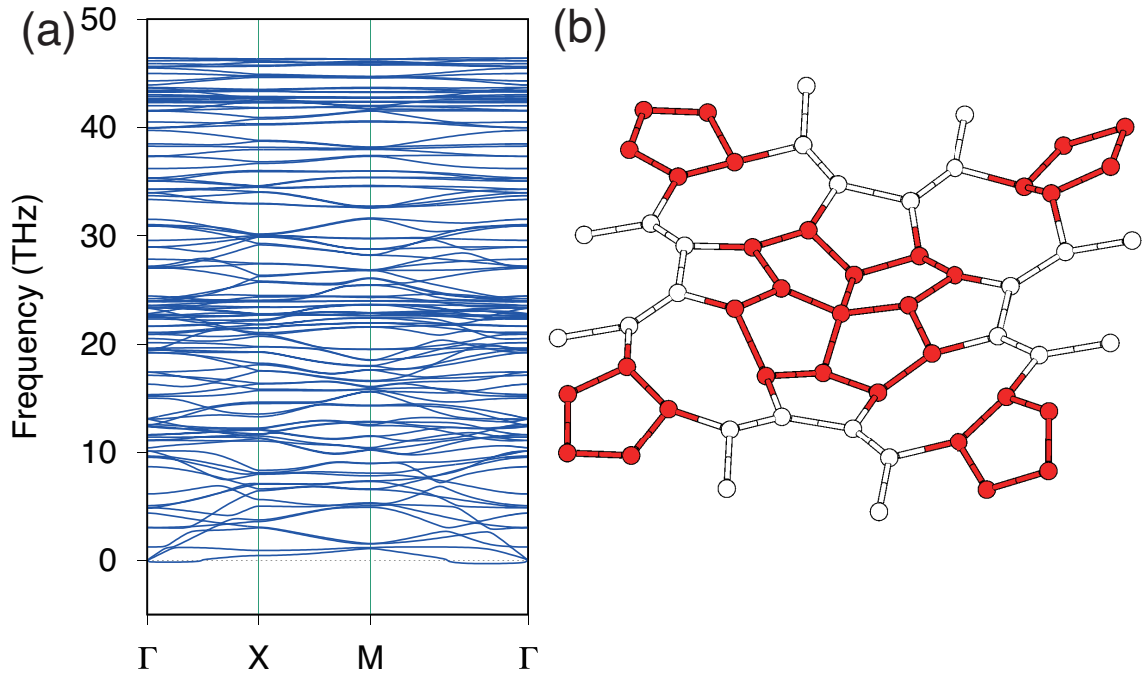

Fig. 2. (a) Phonon dispersion relation of spiro-graphene comprising [5.5.5.5]-fenestratetraene and cyclooctatetraene frameworks. (b) A snapshot of the spiro-graphene comprising [5.5.5.5]-fenestratetraene and cyclooctatetraene frameworks at T = 2000 K after 2 ps of molecular dynamics simulation time. Red and white balls indicate C atoms belonging to [5.5.5.5]-fenestratetraene and cyclooctatetraene frameworks, respectively.

phonon dispersion does not have any soft vibrational modes, confirming its dynamical stability. It should note that small negative (imaginary) phonon frequencies around the Γ point may indicate the dynamic instability of spiro-graphene(5,8). Therefore, appropriate supporting substrates for the synthesis of the spiro-graphene(5,8) sheet are required. The dynami-

cal/thermal stability is also investigated by carrying out ab initio molecular dynamics (MD) simulations implemented in the STATE package. To maintain the temperature, we used the velocity scaling method. We consider a 1×1×1 unit cell with the equidistant 4×4 $\boldsymbol{k}$-meshes for Brillouin integration. Time step for MD calculation is 2 fs. The copolymer retained the initial covalent network topology for 2 ps at $T = 2000$ K [Fig. 2(b)]. Therefore, the phonon dispersion and ab initio MD simulations confirmed that the spiro-graphene(5,8) is thermally and energetically stable once synthesized using appropriate copolymerization processes.

We investigated the formation energy ΔE of a direct copolymerization reaction of [5.5.5.5]-fenestratetraene and cyclooctatetraene into spiro-graphene:

$$\text{fenestratetraene} + \text{cyclooctatetraene} = \text{spiro} - \text{graphene} + 10 \times \text{H}_2 - \Delta E$$

The calculated formation energy was 9.4 eV, which corresponds to the energy cost to extend a covalent network of sp^2 with distorted bond angles. This large formation energy implies that the direct copolymerization of [5.5.5.5]-fenestratetraene and cyclooctatetraene would be difficult to achieve directly. Thus, appropriate intermediates, such as Br-substituted derivatives, are required to achieve polymerization.

The electronic structure of spiro-graphene(5,8) is depicted in Fig. 3. The spiro-graphene is a metal where the dispersive band crosses the Fermi level. A hole pocket is located at the Γ point, whereas an electron pocket emerges at the middle of the Brillouin zone as the strip forms a closed circle. Therefore, the carriers on this metallic C allotrope are both holes and electrons. The squared wave functions of the electronic states near the Fermi level and at the Γ point exhibit a π-state nature, which is totally extended through the covalent network of sp^2 C atoms. The absence of the wave function distribution on sp^3 C atoms can provide an interpretation of the characteristic dispersion relation of the electron states near the Fermi level. All states doubly degenerate along the zone boundary from the X to M. The doubly degenerate bands at the zone boundary are attributed to the band folding of the two-dimensional band of $1/\sqrt{2} \times 1/\sqrt{2}$ face-centered square lattice into the present 1×1 lattice because the π electron network is approximately regarded as a flat topological network. Owing to this band folding , the electronic states near the Fermi level form the Dirac nodal line, as in the case of the spiro-graphene(5,0).

The low-density covalent networks of sp^2 and sp^3 C atoms raise the question of whether the structural phase transition into other structures is possible by applying tensile and compressive strains. To investigate the possibility, we applied biaxial compressive and tensile strains on the spiro-graphene (Fig. 4). The spiro-graphene undergoes a structural phase tran-

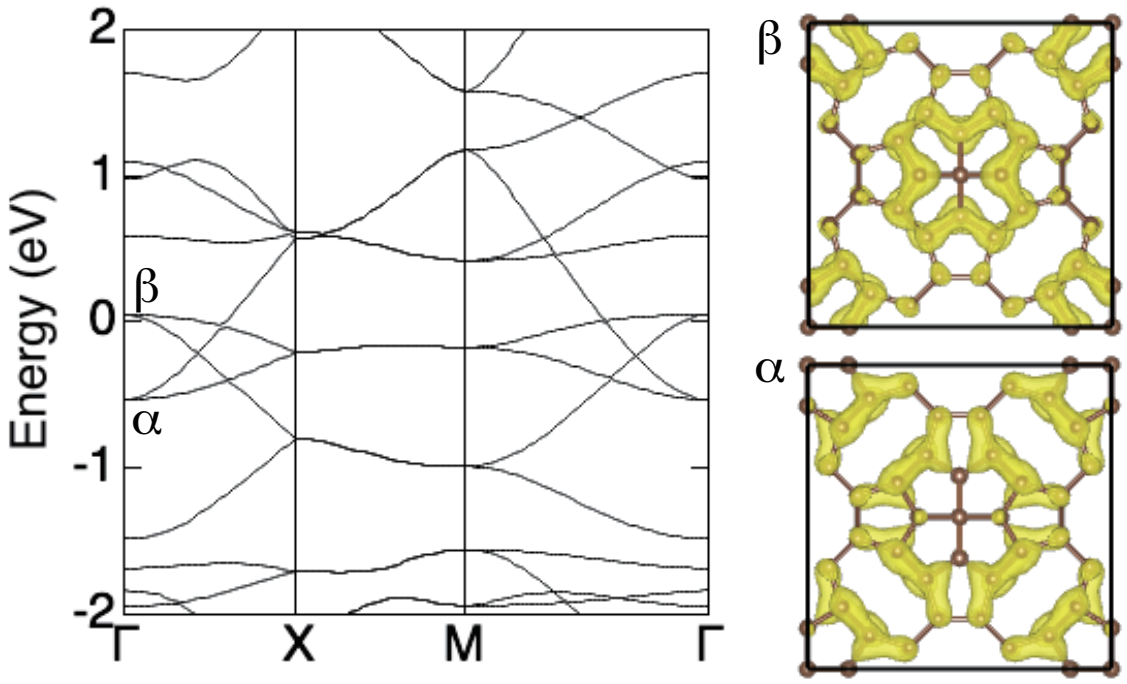

Fig. 3. (a) The electronic band structure of spiro-graphene comprising [5.5.5.5]-fenestratetraene and cyclooctatetraene at and along the high symmetry points and lines. Energies are measured from the Fermi level energy. (b) Isosurfaces of squared wave functions of the electron states near the Fermi level at the Γ point.

sition into another structure under the tensile strain of 0.11 nN. The optimum lattice parameter and the total energy of the phase are 11.80 Å and 0.829 eV/atom, respectively. Under the equilibrium lattice parameter, this new phase has an atomic density of 0.29 atom/Å^2, which is remarkably lower than that of the starting high-density phase.

Figure 5 and Table II show the optimized structure and atomic coordinates of the low-density phase of the spiro-graphene, respectively. The low-density phase is obtained by dissociating the C4–C5 bonds in the high-density phase. Accordingly, the low-density phase consists of two-, three-, and fourfold coordinated C atoms, which results in the large lattice parameters and low density. Bond lengths associated with two-, three-, and fourfold coordinated C atoms are 1.23 Å, 1.38–1.45 Å, and 1.54 Å, respectively, indicating that the network contains all hybridizations of C atoms. The tensile strain dissociated the threefold coordinated C atoms belonging to the cyclooctatetraene unit, whereas the four- and threefold coordinated C atoms in the fenestratetraene unit retain their initial covalent network. Thus, the four fused pentagons in the spiro-graphene are highly robust against external perturbations so that further variations of covalent networks of spiro-graphene are expected. Note that the low-density

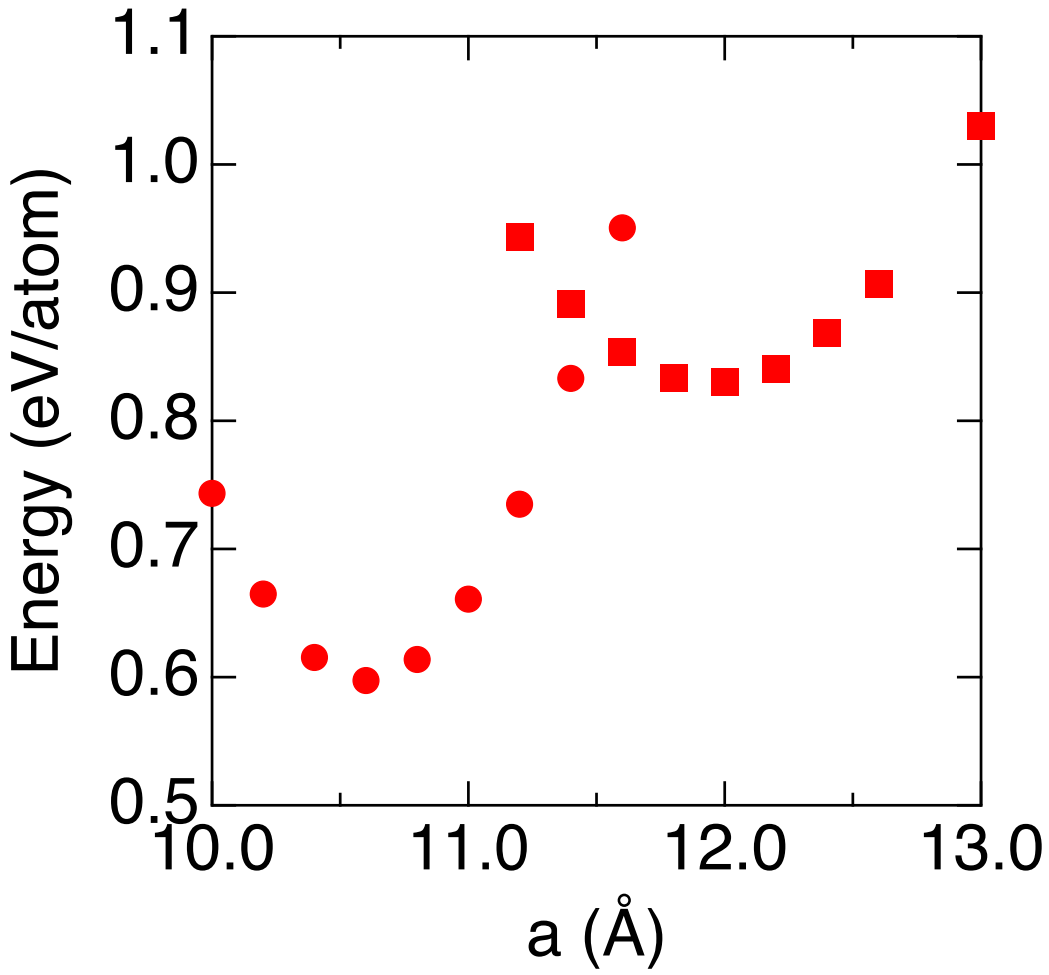

Fig. 4. The relative energy of the spiro-graphene comprising [5.5.5.5]-fenestratetraene and cyclooctatetraene per atom as a function of the lattice parameter, a. Circles and squares indicate the energies of the spiro-graphene without and with twofold coordinated C atoms, respectively. The energy is measured from that of graphene with the equilibrium lattice constant.

phase of the spiro-graphene(5,8) is thermally unstable because it has a negative phonon mode at the Γ point. Therefore, the phase may retain its covalent network on appropriate supporting substrates.

The bond dissociation highly modulates the electronic structure of the spiro-graphene. Figure 6(a) shows the electronic structure and the squared wave functions at the Fermi level and the Γ point of the low-density phase of the spiro-graphene. The low-density phase is also a metal with a peculiar electronic structure at the Fermi level. Although the flat dispersion bands emerge at the Fermi level along the Γ–X line, the electronic states associated with these states are extended through the covalent network with π electronic state nature. Thus,

Table II. Optimized atomic coordinates, lattice constants, and space group symmetry of the low-density phase of the spiro-graphene comprising [5.5.5.5]-fenestratetraene and cyclooctatetraene units. Atom indexes are defined in Fig. 5.

Pmmn	$a = b$ =11.80 Å	c =12.00 Å	
C1	0.000000	0.879852	0.550891
C2	0.103640	0.824384	0.534434
C3	0.175738	0.896337	0.466357
C4	0.284282	0.858040	0.444208
C5	0.141780	0.715703	0.556674
C6	0.000000	0.000000	0.500290
C7	0.120338	0.000000	0.449818

the flat band is not caused by the localized π electrons but by the delicate balance of the electron transfer among π electrons on the network. According to these flat bands at the Femi level, the low-density phase exhibits spin polarization as its ground and metastable states [Fig. 6(b) and 6(c)]. The total energies of the antiferromagnetic state and ferromagnetic state are lower than that of the nonmagnetic state by 96 meV/unit cell and 4 meV/unit cell, respectively. Therefore, the low-density phase of the spiro-graphene(5,8) is a possible magnetic all C material without edges and defects.

4. Conclusion

We theoretically designed a two-dimensional covalent network of sp^2 and sp^3 C atoms as a metallic C allotrope with the Dirac nodal lines just below the Fermi level. The network consists of [5.5.5.5]-fenestratetraene and cyclooctatetraene frameworks by copolymerizing these hydrocarbon molecules with dehydrogenation so that it could be classified as a spiro-graphene related material. Because the network contains [5.5.5.5]-fenestratetraene and an octagon, this spiro-graphene is a low atomic-density material with a density of 0.374 atom/Å^2, which is lower than those of the spiro-graphene comprising spiro[4,4]nonatetraene (0.411 atom/Å^2) and graphene (0.661 atom/Å^2). Our DFT calculations demonstrated that this spiro-graphene has a total energy of approximately 600 meV/atom with respect to that of graphene, which is close to that of other spiro-graphene materials, owing to its rippled covalent networks. We also confirm that this spiro-graphene is thermally stable by conducting phonon calculations and ab initio MD simulations. Furthermore, the spiro-graphene undergoes a structural phase transition to the low-density phase under the biaxial tensile strain of 0.11 nN. The low-density

phase has an atomic density of 0.29 atom/Å^2 owing to the formation of sp C atoms by the bond dissociation of sp^2 C atoms belonging to the octagonal rings. Despite the low-density phase being thermally unstable owing to the soft vibrational mode at the Γ point, the spiro-graphene of the low-density phase has peculiar flat dispersion bands at the Fermi level and along the Γ–X line. Accordingly, the low-density phase has spin-polarized states where the polarized electrons are ferromagnetically and antiferromagnetically aligned with a π state nature extended through the sp and sp^2 C atoms in the network. Therefore, the low-density phase of the spiro-graphene is an all-carbon magnetic material without containing unsaturated C atoms associated with the edges and defects.

Acknowledgment

The authors thank the Japan Science and Technology Agency, Core Research for Evolutionary Science and Technology (JST-CREST; Grant Nos. JPMJCR1715 and JPMJCR20B5) and the Japan Society for the Promotion of Science, Grants-in-Aid for Scientific Research (JSPS KAKENHI; Grant Nos. JP21H05233, JP21H05232, JP21K14484, JP20K22323, JP20H00316, JP20H02080, JP20K05253, and JP20H05664), the Joint Research Program on Zero-Emission Energy Research, Institute of Advanced Energy, Kyoto University, and the University of Tsukuba Basic Research Support Program (S). Part of the calculations was performed on an NEC SX-Ace at the Cybermedia Center at Osaka University.

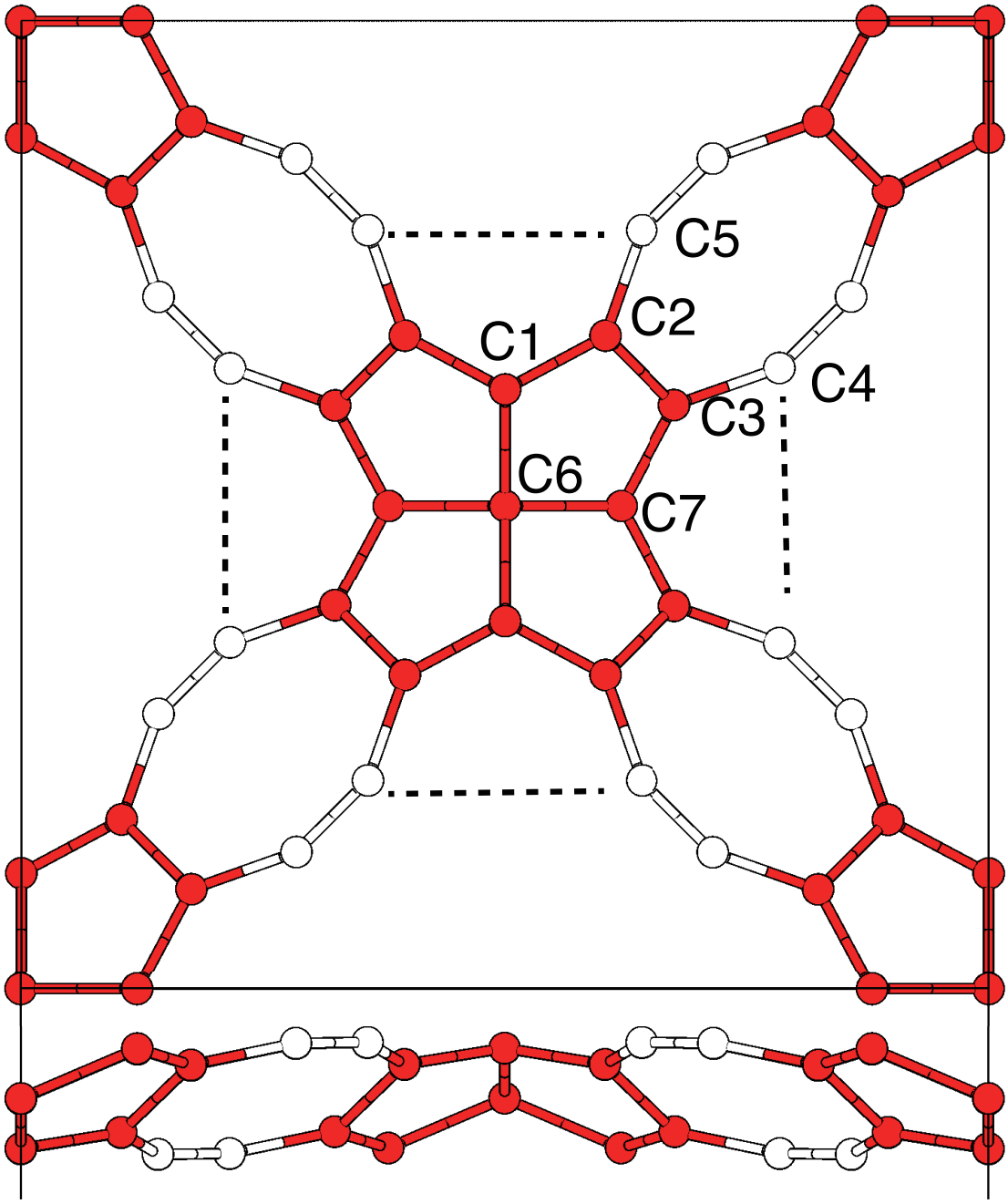

Fig. 5. Top and side views of an optimized atomic structure of the low-density phase of the spiro-graphene comprising [5.5.5.5]-fenestratetraene and cyclooctatetraene frameworks. Red and white atoms indicate C atoms originating from [5.5.5.5]-fenestratetraene and cyclooctatetraene frameworks, respectively. The solid square indicates the unit cell boundary, and the indexes indicate independent atomic sites under the symmetry of *Pmmn*. Dotted lines denote the bonds dissociated under the structural transition to the low-density phase.

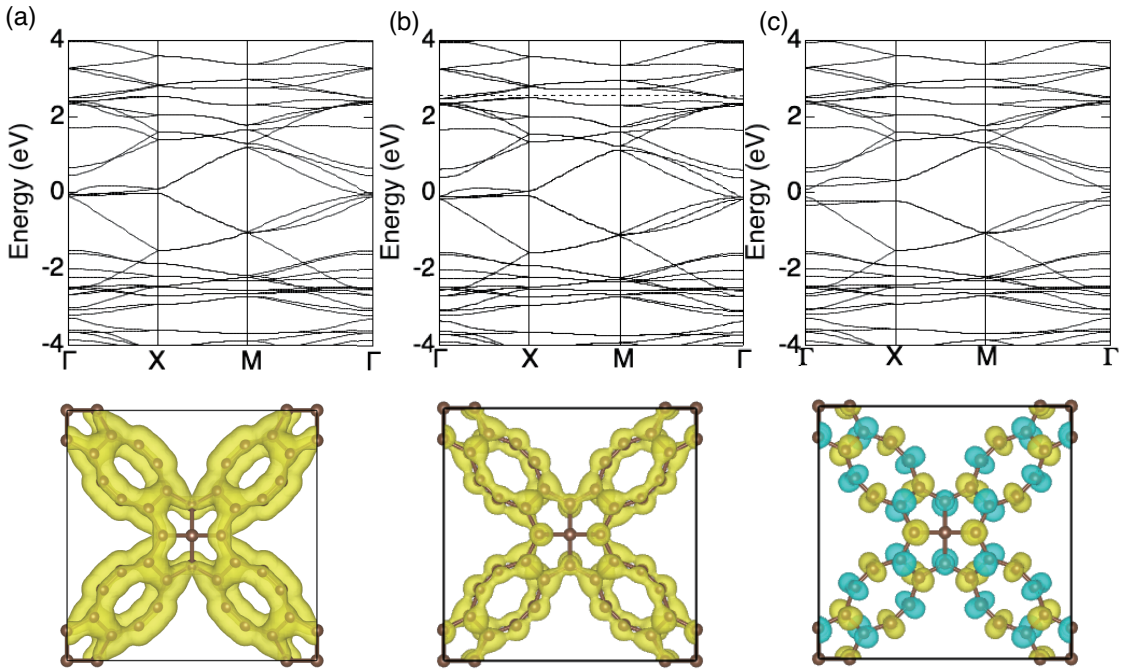

Fig. 6. (a) The electronic band structure and isosurfaces of the squared wave function at the Fermi level and the Γ point of the low-density phase of spiro-graphene without a spin degree of freedom. The electronic band structure and isosurfaces of the spin density of the low-density phase of spiro-graphene with (b) ferromagnetic and (c) antiferromagnetic states. Energies are measured from the Fermi level energy. Solid and dotted lines denote the energy bands of *alpha* and β spin states, respectively. Note, the dotted lines almost overlap with the solid lines owing to the small exchange splitting between α and β states. Yellow and cyan surfaces of the charge density of α and β spin components, respectively.

References

1) G. S. Painter and D. E. Ellis, Phys. Rev. **1**, 4747 (1970).

2) F. Bassani and G. P. Parravicini, Nuovo Cimento B **50**, 95 (1967).

3) M. Posternak, A. Baldereschi, A. J. Freeman, E. Wimmer and M. Weinert, Phys. Rev. Lett. **50**, 761 (1983).

4) K. S. Novoselov, A. K. Geim, S. V. Morozov, D. Jiang, M. I. Katsnelson, I. V. Grigorieva, S. V. Dubonos, and A. A. Firsov, Nature **438**, 197 (2005).

5) Y. Zhang, Y. -W. Tan, H. L. Stormer, and P. Kim, Nature **438**, 201 (2005).

6) X. Du, I. Skachko, F. Duerr, A. Luican, and E. Y. Andrei, Nature **462**, 192 (2009).

7) K. I. Bolotin, F. Ghahari, M. D. Shulman, H. L. Stormer, and P. Kim, Nature **462**, 196 (2009).

8) N. Shima and H. Aoki, Phys. Rev. Lett. **71**, 4389 (1993).

9) Y. Ma, P. O. Lehtinen, A. S. Foster, and R. M. Nieminen, New J. Phys. **6**, 68 (2004).

10) H. Amara, S. Latil, V. Meunier, Ph. Lambin, and J.-C. Charlier, Phys. Rev. B **76**, 115423 (2007).

11) M. M. Ugeda, I. Brihuega, F. Hiebel, P, Mallent, J.-Y. Veuillen, J. M. G.-Rodriguez, and F. Yndurain, Phys. Rev. B **85**, 121402(R) (2012).

12) M. Sakurai, Y. Sakai, and S. Saito, J. Phys.: Conf. Ser. **302**, 012018 (2011).

13) M. Maruyama, N. T. Cuong, and S. Okada, Carbon **109**, 755 (2016).

14) M. Fujita, K. Wakabayashi, K. Nakada, and K. Kusakabe, J. Phys. Soc. Jpn. **65**, 1920 (1996).

15) K. Nakada, M. Fujita, G. Dresselhaus, and M. S. Dresselhaus, Phys. Rev. B **54**, 17954 (1996).

16) Y. Miyamoto, K. Nakada, and M. Fujita, Phys. Rev. B **59**, 9858 (1999).

17) S. Okada and A. Oshiyama, Phys. Rev. Lett. **87**, 146803 (2001).

18) K. Kusakabe, K. Wakabayashi, M. Igami, K. Nakada, and M. Fujita, Mol. Cryst. Liq. Cryst. **305**, 445 (1997).

19) J. Fernández-Rossier and J. J. Palacios, Phys. Rev. Lett. **99**, 177204 (2007).

20) O. V. Yazyev and S. G. Louie, Phys. Rev. B **81**, 195420 (2010).

21) S. Okada, T. Kawai, and K. Nakada, J. Phys. Soc. Jpn. **80**, 013709 (2011).

22) M. Maruyama, and S. Okada, Appl. Phys. Express **6**, 095101 (2013).

23) M. Maruyama, and S. Okada, Carbon **125**, 530 (2017).

24) L. Zhi and K. Müllen, J. Mater. Chem. **18**, 1472 (2008).

25) J. Cai, P. Ruffieux, R. Jaafar, M. Bieri, T. Braun, S. Blankenburg, M. Muoth, A. P. Seitsonen, M. Saleh, X. Feng, and K. Müllen, Nature **466**, 470 (2010).

26) L. Chen, Y. Hernandez, X. Feng, and K. Müllen, Angew. Chem. Int. Ed. **51**, 7640 (2012).

27) A. P. Côté, A. I. Benin, N. W. Ockwig, M. O'Keeffe, A. J. Matzger, and O. M. Yaghi, Science **310**, 1166 (2005).

28) F. J. Uribe-Romo, J. R. Hunt, H. Furukawa, C. Klöck, M. O'Keeffe, and O. M. Yaghi, J. Am. Chem. Soc. **131**, 4570 (2009).

29) T. Ben, H. Ren, S. Ma, D. Cao, J. Lan, X. Jing, W. Wang, J. Xu, F. Deng, J. M. Simmons, S. Qiu, and G. Zhu, Angew. Chem. Int. Ed. **48**, 9457 (2009).

30) W. Lu, D. Yuan, D. Zhao, C. I. Schilling, O. Plietzsch, T. Muller, S. Bräse, J. Guenther, J. Blümel, R. Krishna, Z. Li, and H.-C. Zhou, Chem. Mater. **22**, 5964 (2010)

31) Y. Fujii, M. Maruyama, K. Wakabayashi, K. Nakada, and S. Okada, J. Phys. Soc. Jpn. **87**, 034704 (2018).

32) Y. Fujii, M. Maruyama, and S. Okada, Jpn. J. Appl. Phys. **58**, 085001 (2019).

33) B. Ram and H. Mizuseki, Carbon **137**, 266 (2018).

34) B. Ram and H. Mizuseki, Carbon **158**, 827 (2020).

35) S. Okada, N. T. Cuong, Y. Gao, and M. Maruyama, Carbon **185**, 404 (2021).

36) R. Mitschka, J. Oehldrich, K. Takahashi, J. M. Cook, U.Weiss, and J. V. Silverton, Tetrahedron **37**, 4521 (1981).

37) M. N. Deshpande, M. Jawdosiuk, G. Kubiak, M. Venkatachalam, U. Weiss, and J. M. Cook, J. Am. Chem. Soc. **107**, 4786 (1985).

38) M. Venkatachalam, M. N. Deshpande, M. Jawdosiuk, G. Kubiak, S. Wehrli, J. M. Cook, and U. Weiss, Tetrahedron **42**, 1597 (1986).

39) D. Kuck, A. Schuster, and R. A. Krause, J. Org. Chem. **56**, 3472 (1991).

40) P. Hohenberg and W. Kohn, Phys. Rev. **136**, B864 (1964).

41) W. Kohn and L. J. Sham, Phys. Rev. **140**, A1133 (1965).

42) Y. Morikawa, K. Iwata, and K. Terakura, Appl. Surf. Sci. **169-170**, 11 (2001).

43) A simulation tool for atom technology (STATE): https://state-doc.readthedocs.io/en/latest/index.html

44) P. Giannozzi et al., J. Phys.: Condens. Mater. **21**, 395502 (2009).

45) J. P. Perdew, K. Burke, and M. Ernzerhof, Phys. Rev. Lett. **77**, 3865 (1996).

46) D. Vanderbilt, Phys. Rev. B **41**, 7892 (1990).

47) A. Togo and I. Tanaka, Scr. Mater. **108**, 1 (2015) .